IEEE Access
Multidisciplinary ⋮ Rapid Review ⋮ Open Access Journal

Received 5 January 2024, accepted 25 January 2024, date of publication 30 January 2024, date of current version 8 February 2024.

Digital Object Identifier 10.1109/ACCESS.2024.3359907

RESEARCH ARTICLE

Numerical Design of 0.99 Numerical Aperture Planar Metalens for High Spatial Resolution Terahertz Imaging

HUU LAM PHAN[1,2], KWANGSOO KIM[3], JONG-MO SEO[4], (Member, IEEE), AND KYO-IN KOO[5], (Member, IEEE)

[1]Laboratory for Computational Mechanics, Institute for Computational Science and Artificial Intelligence, Van Lang University, Ho Chi Minh City 70000, Vietnam
[2]Faculty of Mechanical–Electrical and Computer Engineering, School of Technology, Van Lang University, Ho Chi Minh City 70000, Vietnam
[3]Department of Electronic Engineering, Hanbat National University, Daejeon 34158, Republic of Korea
[4]Department of Electrical and Computer Engineering, Seoul National University, Seoul 08826, Republic of Korea
[5]Major of Biomedical Engineering, Department of Electrical, Electronic, and Computer Engineering, University of Ulsan, Ulsan 44610, Republic of Korea

Corresponding authors: Jong-Mo Seo (callme@snu.ac.kr) and Kyo-In Koo (kikoo@ulsan.ac.kr)

This work was supported by the Korean Medical Device Development Fund, Republic of Korea, under Grant KMDF PR 20210527 00062021-01.

ABSTRACT Terahertz (THz) wave imaging has potential features for medicine, such as cancer detection. Nevertheless, traditional lenses are heavy, bulky, low spatial resolution, and difficult to integrate. Recently, metasurface has emerged as a compelling approach for achieving lightweight, ultrathin, and easy integration. Although many THz metasurface lenses have been proposed for the wave-focusing applications, there are a few THz metalenses that are polarization insensitive and have a high spatial resolution for THz imaging. In this paper, an ultra-thin, planar, polarization-independent, and high numerical aperture metalens has been proposed using double split-ring resonator (DSRR) structures for high-resolution THz wave focusing. The combination method of the propagation phase (adjusting the diameter of the outer ring of the DSRR) and the geometric phase (changing the slit of the DSRR) is applied to build the unit cell library including eight DSRRs, which can cover the full phase from 0 to 2π and is independent with the polarization of the incident wave. By arranging the DSRRs into the concentric rings on a thin substrate, an ultrathin, polarization-insensitive, and high numerical aperture metalens is designed with a thickness of 0.55λ, a focal length of 660 μm (4λ), radius of 4.678 mm ($28.35\ \lambda$), and numerical aperture of 0.99 that can work at 1.82 THz (wavelength (λ) of 165 μm). The designed metalens with a near-unity numerical aperture achieves a high spatial resolution of 89 μm (0.54λ), which can produce high-quality images. It means that the proposed metalens can resolve the microscale features separated by a sub-wavelength distance ($< 90\ \mu$m). Therefore, the suggested metalens can serve as an objective lens for the miniaturized microscopy, opening a new avenue for microscopic THz imaging and showing potential usage in tiny THz imaging systems for cancer detection applications.

INDEX TERMS High numerical aperture, high spatial resolution, metasurface lens, metalens, terahertz.

I. INTRODUCTION

Terahertz (THz) radiation has attracted increasing interest in various fields such as communication [1], material characterization [2], biological sensing [3], and imaging systems [4], [5], [6], [7] due to its unique characteristics such as nonionizing, noninvasive, phase-sensitive to polar substances, spectral fingerprinting, coherent detection, high resolution, and high penetration capabilities [8]. In the last decade, the terahertz imaging system has been developed for

The associate editor coordinating the review of this manuscript and approving it for publication was Bilal Khawaja.

medical applications such as cancer detection [9], [10]. However, the spatial resolution of these systems is a millimeter scale that is vastly larger than the wavelength (λ). Operating at higher frequencies (shorter wavelength) may enhance the resolution. For example, Joseph et al. proposed a terahertz transmission imaging system, including a focusing lens and a short focal length off-axis parabolic mirror for detection of the area of nonmelanoma skin cancer tissue at a frequency of 1.63 THz. The system only provides a terahertz transmission image of nonmelanoma skin cancers with a spatial resolution of 0.49 mm (2.61λ) [11]. Another type of terahertz imaging system using the reflection mode through the off-axis parabolic mirror for breast cancer detection at 1.89 THz was presented by Peter et al. However, the system exhibited a millimeter scale spatial resolution image of 1.8 mm (6.53λ) [12]. Bowman et al. reported another terahertz reflection imaging system for breast tumor tissue detection with 1.75 THz. The terahertz reflection images of tumor tissue were acquired with a spatial resolution of 200 μm (1.17λ) [13]. The spatial resolutions of these systems are still larger than one wavelength, which indicates low spatial resolution. This limits the ability to precisely detect the cancer margin [14]. Therefore, enhancing spatial resolution under a sub-wavelength scale is highly desirable in medical applications.

A variety of techniques have been reported to enhance the spatial resolution to the sub-wavelength scale [15], [16], [17], [18]. For example, an aperture-less terahertz scanning near-field optical microscopy has been demonstrated to achieve high spatial resolution (λ/3000) [19]. This method used a nano-sharp metal tip instead of resolving aperture and the scattering of the incident wave is measured. However, this method invariably suffers from significant signal attenuation because of confined to a nano metal tip and its scattering. In addition, this technique requires a long scanning time, strong emitters, and highly sensitive detectors. Another technique using lens-less holography is shown to obtain the sub-wavelength scale for terahertz imaging resolution [20]. However, to precisely resolve the inverse ill-posed problems of holography, this technique needs complicated computations [21].

Recently, enlarging the lens aperture is a promising method for achieving sub-wavelength scale resolution for terahertz imaging. However, enhancing the numerical aperture (NA) of the spherical lens (conventional refractive lens) is ineffective because the spherical aberration phenomenon is significantly increased. To overcome the limitation of the spherical lens, the aspherical refractive lens is proposed [17], [18]. Increasing the NA (0.86) of the aspherical refractive lens could be obtained the sub-wavelength scale resolution (0.95λ with $\lambda = 300$ μm) [18]. Nevertheless, to manufacture the aspherical refractive lens, more complex fabrication techniques are required than a conventional spherical refractive lens. In addition, conventional refractive lenses reshape the wavefront of light based on gradual phase accumulation along a curved optical route [22]. To cover the full phase, thicknesses of spherical/aspherical refractive lenses are recommended to be substantially larger than the incident wavelength, which leads to the bulkiness of the lens. Therefore, it is a challenge to fabricate a conventional refractive lens with a high NA and short focal length, particularly for applications, such as portable and wearable devices. To overcome these limitations of conventional lenses, diffractive types of terahertz lenses have been proposed [23], [24], [25], but thicknesses of lenses were still above 2 millimeters [25].

In recent years, a metasurface has been recommended as a potential approach for modulating the phase, amplitude, and polarization of light at the sub-wavelength scale [26], [27], [28], [29], [30]. Unlike conventional lenses, the metasurface can break dependence on the propagation effect by introducing phase discontinuities using highly integrated micro-nano structured surfaces [31], [32], [33]. Consequently, the metasurface enables to achieve the required phase shifts covering the full range from 0 to $2\boldsymbol{\pi}$ over a wavelength propagation distance, which makes it one of the appropriate options for miniaturization and integration of photonic systems [33], [34]. Thanks to these advantages, the metasurface has been applied to various applications including holograms [35], [36], [37], cloak [38], [39], and biosensing [40], [41] as well as metalenses [42], [43], [44], [45]. The metalens is the significant application of the metasurface due to its outperforming optical properties [46], [47]. Compared with the traditional terahertz lens, the terahertz metalens can satisfy the growing demand for high-integration, low-cost miniature optical systems, without spherical aberration because of its flat structure [48]. To date, transmissive terahertz metalens based on dielectric material have attracted much interest of researchers due to achieving high focusing efficiency [49], [50], [51], [52]. However, the thickness of these devices was still over the working wavelength because of using the block meta-atom structure. Meanwhile, plasmonic metalenses based on plasmonic metasurface have low focusing efficiency due to ohm loss of metallic layer, but they showed more compact shapes and wider dynamic ranges compared with the all-dielectric metalenses [53], [54], [55], [56], [57]. Although much effort has been put into the designing metalens, these above terahertz metalenses feature low NA (less than 0.7), resulting in poor spatial resolution that is still larger than the operating wavelength. In addition, some metalenses are only acceptable for linearly polarized (LP) incident waves [49], [53], [54], [55], [56], [57], whilst others are only used with circularly polarized (CP) incoming wave [50], [51], [58]. As a result, the aforementioned metalenses are sensitive to the polarized incident wave, which restricts their practical applications. Therefore, developing a lens with ultrathin structure, polarization insensitivity, and especially high spatial resolution is essential for miniaturizing the THz imaging system and precise detection of cancer margin.

To overcome the shortcomings of the traditional lens and the existing metalens, in this paper, a planar terahertz metalens using an array of double-split-ring resonators (DSRRs)

with high numerical aperture is proposed for a terahertz imaging system in cancer detection applications. Eight different DSRRs were designed as elements of an array to manipulate the phase with a similar amplitude. Using the eight DSRRs, a concentric-circle-shaped array was designed on a polyimide substrate to form the proposed metalens. The advantages of this metalens are pointed out as follows:

- Simple design of planar, lightweight, and polarization-insensitive metalens based on the DSSRs structure. It is suitable for the miniaturized system and can easily integrate into the current image sensor.
- The proposed metalens has a near-unity numerical aperture of 0.99 that operates at a frequency of 1.82 THz.
- The designed metalens achieves a high spatial resolution (0.54λ), which is very close to the theoretical diffraction limit, that can produce high-quality images. It provides an excellent choice for the THz imaging system for precise cancer margin detection applications.

This paper is organized as follows: Section II concentrates on the proposed metalens design and how to simulate the designed metalens that operates efficiently at THz frequency. Section III shows the performances of the suggested metalens and compares them to the existing state-of-the-art THz metalens. Finally, this work is concluded in Section IV.

II. DESIGN AND METHODS

The fundamental aspects of polarization manipulation of metasurface result from the cross-coupling of electric and magnetic field resonances in the presence of an incoming wave with a certain polarization state. To obtain polarization-independent wavefront control, the meta-atom with diagonal symmetric structure of the metasurface needs to be tailored to the cross-coupling effects. In the previous reports, the many diagonal symmetric structures such as V-shape, C-shape, U-shapes, L-shape have been demonstrated to achieve the independent polarization of incident [59], [60]. In this paper, a DSRR with diagonal symmetric structure is proposed to obtain the polarization independence of the transmitted terahertz wave, as described in Fig. 1. Electromagnetic wave impinging on the DSRR produces cross-polarized scattering waves. In addition, a phase abruption between the metasurface and the incident wave is formed as well. Generally, there are three phase modulation principles to perform full phase control of metasurfaces, including propagation phase, geometric phase, and combination of these two above techniques [61]. For the propagation phase method, the phase response is covered from 0 to 2π by adjusting the structural parameters of the unit cell with a fixed angular direction. On the other hand, the geometric phase technique can cover the full phase control by changing the orientation angle (θ) of the identical unit cell. According to ref. [48], [62], the full phase modulation from 0 to 2π is controlled by rotating the θ of the unit cell from 0 to π. Therefore, only one unit cell is required when designing a metasurface based on the geometric phase. However, this method is only suitable for

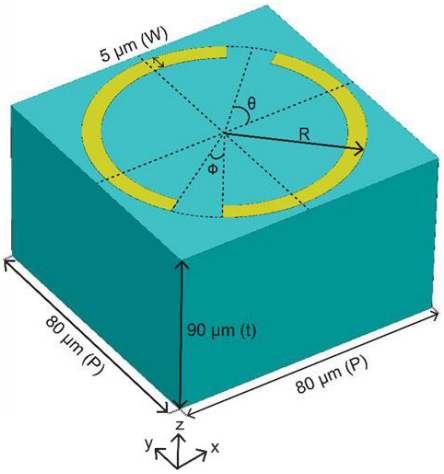

FIGURE 1. The schematic views and parameter of the DSRR on the surface of the polyimide substrate.

circularly polarized incident waves. It is clear that the two above phase modulation methods only work for LP or CP, respectively. It makes the limitation in the design of general polarization independent metalens. To overcome this limitation, combining the propagation and geometric phase is one viable technique [59], [61]. In the combination method, the phase response is defined as two parts: the first is the angle independent phase, which is only present through the propagation phase, and the second is the angle dependent phase based on the geometric phase.

Therefore, the combination method of the propagation phase and the geometric phase is applied to design the metasurface that can cover full phase from 0 to 2π in this study. For the first term, using the propagation phase technique, the phase response is covered from 0 to π by studying the change in the ring radius (R) of the proposed structure. The surface current travels a longer path of the resonator with a larger ring radius, which causes the lower corresponding frequency at the abrupt phase (π) point. In addition, after the phase (π) point, the phase spectra for the various resonators remain parallel to one another, as shown in Fig. S1(b). Hence, a phase (0 - π) can be achieved at the fixed operation frequency point through changing the outer radius. For the second part, using the geometric phase method, the remained phase (π - 2π) is obtained at the fixed operation frequency point by rotating the orientation angle (θ) of 90°. To evaluate our design, CST Microwave StudioTM (3DS Company, U.S.A) was employed. In this case, the unit cell boundary conditions in the x and y axis directions, and the open boundary conditions in the z axis direction are utilized for the designed unit cell structure. The S-parameters of the designed unit cell structure can be achieved by the Floquet-port excitation to compute the transmission efficiency.

In this work, we design the metalens operating at the frequency of 1.82 THz for the cancer detection application. Specifically, a unit of the DSRR was designed with 0.2 μm thick aluminum on a 90 μm thick polyimide substrate (t) with an 80 μm lattice period (p), as shown in Fig. 1. The aluminum

TABLE 1. The design parameters of the proposed 8 DSRR units and their phase shift abilities.

DSRR unit cell name	Outer radius (R, unit: μm)	Direction angle of the slit (θ)	Phase shift abilities (rad)
DSRR unit 1	37	45°	0
DSRR unit 2	33.5	45°	$\pi/4$
DSRR unit 3	27.5	45°	$\pi/2$
DSRR unit 4	22	45°	$3\pi/4$
DSRR unit 5	37	135°	π
DSRR unit 6	33.5	135°	$5\pi/4$
DSRR unit 7	27.5	135°	$3\pi/2$
DSRR unit 8	22	135°	$7\pi/4$

was modeled as a lossy metal with a conductivity of 3.56×10^7 S/m. The polyimide was modeled as a loss-less dielectric with a dielectric constant of 3.5. The width of the ring and the central angle of the slit in the DSRR unit were fixed as 5 μm (w) and 21° (Φ), respectively. The ring radius and slit direction of the DSRR unit varied to modulate wavefront. Table 1 describes the specific design parameters and their phase shift analyzed numerically at the frequency of 1.82 THz (165 μm). At the slit direction of 45° (θ), the ring radii (R) were designed with 37, 33.5, 27.5, and 22 μm to achieve 0, $\pi/4$, $\pi/2$, and $3\pi/4$ phase shift abilities, respectively. To achieve π, $5\pi/4$, $3\pi/2$, and $7\pi/4$ phase shift abilities, the slit direction was changed as 135° (θ) and the ring radii (R) were composed as 37, 33.5, 27.5, and 22 μm correspondingly. The transmittance amplitudes range from 0.18 to 0.22 with a mean value of 0.2, as described in Fig. S1(a) (see in Section I of Supplementary file). Their phase shift abilities covered well from 0 to 2π with $\pi/4$ span, as shown in Fig. S1(b) (see in Section I of Supplementary file). Therefore, these phase modulation properties of the proposed eight DSRR units meet the demands of phase coverage over the whole 2π range and identical amplitudes to design a planar metalens, which are similar to those of the V-shaped [53] and the C-shaped [57].

Using the proposed eight units, a DSRR array was designed to implement a focusing lens at 1.82 THz (165 μm). In order to focus a wave having the wavelength $\boldsymbol{\lambda}$ into the focal length f, the required phase shift $\psi(x)$ at a distance of x from the center of the metalens is as follows [63]:

$$\boldsymbol{\psi}(\mathbf{x}) = \frac{2\pi}{\boldsymbol{\lambda}}\left(\sqrt{\mathbf{f}^2+\mathbf{x}^2}-\mathbf{f}\right) \tag{1}$$

To attain metalens focusing at 1.82 THz (corresponding to wavelength 165 μm), the focal length (f) is selected as 660 μm. The phase shifts of our eight resonant units are preset so that we can calculate the distance (x) from the lens center using Eq. (1). In this simulation, this proposed metalens is analyzed by time-domain solvers. In addition, the open boundary conditions were used in the x-, y-, and z-axis directions of the proposed metalens. A plane wave with XLP propagating along the positive z- axis direction was applied as excitation. Good agreement between CST software simulations and experimental results of terahertz metalens was recently reported [63], [64]. Therefore, the simulation

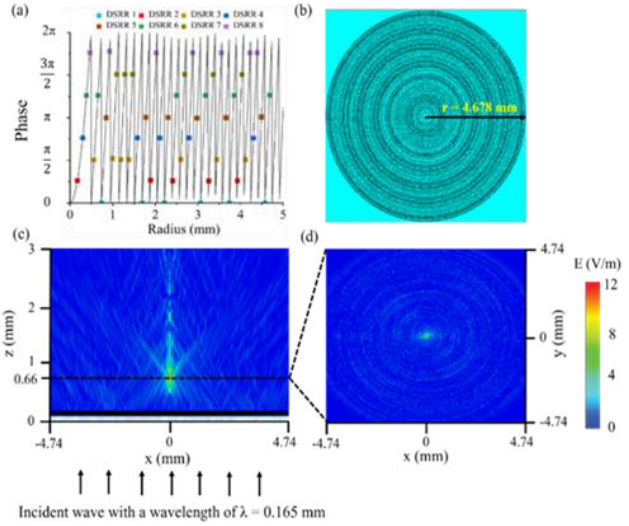

FIGURE 2. (a) The blue solid curve shows the required phase change at the surface and the distance to the center of the lens, and the colorful square points indicate the phase changes provided by the different DSRR units under XLP incident wave with a wavelength of 165 μm (1.82 THz) and focal length of 660 μm. (b) The design of the proposed metalens consists of 48 coaxial DSRR unit rings in a radius of 4678 μm. (c) The simulated electric field intensity distribution of the cross-polarized terahertz wave at 165 μm (1.82 THz) on the xz-planes. (d) The simulated distribution of the electric field intensity is mapped on the xy-plane.

method of CST Microwave Studio™ software is also utilized in this work.

III. RESUTLS AND DISCUSSION

Fig. 2a shows the required phase shift with respect to the distance from the lens center when the wavelength (λ) is set as 165 μm (1.82 THz) and the focal length (f) as 660 μm in Eq. 1 as discussed above. The colorful squares in Fig. 2a indicate the corresponding DSRR units with respect to the required phase shifts based on the phase shift abilities in Table 1. Based on these colorful squares, the DSRR unit number and the distance were selected and arranged in order, as described in Supplementary Section II, so that the metalens was designed as shown in Fig. 2b. The specific number of unit cells to design the proposed metalens is presented in section II of the Supplementary file.

Numerical analysis of the designed metalens shows that the electric field generated around 660 μm above from the metalens surface as expected (Fig. 2c). NA was calculated as 0.99 using the below formula [65]:

$$\mathbf{NA} = \mathbf{sin}(\mathbf{tan}^{-1}\frac{r}{f}) \tag{2}$$

where r is the radius of metalens and f is the focal length. The electric field in the focal plane was distributed uniformly well, as shown in Fig. 2d. As expected, the focus size is rather small, which is in the sub-wavelength scale with an FWHM of 89 μm (0.54λ) (see the Fig. S2 and Fig. S3). Furthermore, Fig. S2 and Fig S3 show that the metalens with higher NA can generate a higher spatial resolution, as described in Section III

TABLE 2. The performance comparison of the other studies to this work.

Reference	Operating wavelength (λ)	Method to enhance spatial resolution	NA	Focal spot size FWHM (μm)
Chernomyrdin et al., 2017 [18]	300 μm	Increasing numerical aperture aspherical lens	0.84	0.95λ
Pham et al., 2017 [14]	2400 μm	Combine spherical lens with a cube and two off-axis parabolic mirror	0.75	0.55λ
		Only high numerical aperture spherical lens	0.75	1.3λ
Li et al., 2019 [66]	1000 μm	Only high numerical aperture aspherical lens	0.9	0.54λ
This work	**165 μm**	**Increasing numerical aperture metasurface lens**	**0.99**	**0.54λ**

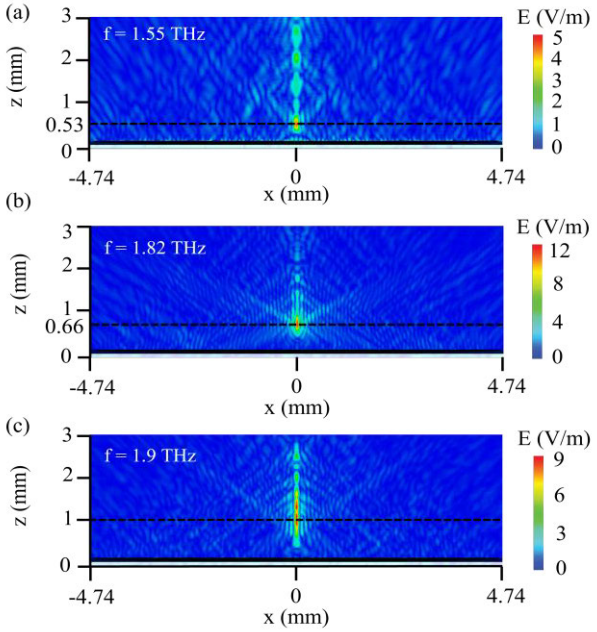

FIGURE 3. (a)-(c) The simulated intensity distribution of the transmitted light via the proposed metalens at different frequencies of 1.55 THz, 1.82 THz, and 1.9 THz, respectively.

of the Supplementary file. Here, we see that the background signals are mostly impacted by co-polarized transmission in Figs. 2(c) and (d).

Table 2 presents the performance comparison of the other studies to this work. Compared to other techniques, the increasing NA of metalens also achieves a sub-wavelength spatial resolution (near-half wavelength). It means that the proposed metalens may provide a high resolution for terahertz imaging system. Furthermore, the proposed metalens is more compact than the aspherical lens. Therefore, it is suitable for compact terahertz imaging systems.

In addition, Fig. S1(b) shows the phase spectrums stay parallel to each other in the frequency range of 1.55 THz ($\boldsymbol{\lambda = 193\mu m}$) to 1.9 THz ($\boldsymbol{\lambda = 157\mu m}$). This implies that the designed units can keep the phase gradient in the broadband, leading to the realization of the broadband focusing. To evaluate the broadband focusing properties of the above DSRR metalens, the incident waves with the frequency of 1.55 THz and 1.9 THz impinge to the above DSRR metalens. Fig. 3 illustrates the high focusing qualities at these frequencies that the above DSRR metalens shows highly broadband performance under XLP incident wave. As expected, the strongest focus with large intensity is achieved at the 1.82 THz incident wave, since the metasurface unit cell is optimally designed for this specific wavelength. However, the focal length of the proposed metalens is changed under the incident wave with 1.55 THz and 1.9 THz. Because, according to Eq. (1), modifying the frequency of the incident wave while maintaining the position of the unit cells changes the corresponding required phase of the unit cells. It leads to changing the focal length of the proposed metalens. Specifically, the focal length is 660 μm at 1.82 THz while the focal lengths are 530 μm and 1000 μm at 1.55 THz μm and 1.9 THz, respectively, as shown in Fig. 3. Therefore, the focal length of the proposed design can be dynamically manipulated by adjusting the incident wavelength change.

Furthermore, due to the symmetric design of the DSRR unit cells and symmetrical axis's orientation angle of 45° or 135°, the proposed metalens is insensitive to polarized incident wave [59]. To demonstrate the independent polarization property, the proposed metalens is exposed to the XLP, YLP, LCP, and RCP of incident light, as shown in Fig. 4 and Fig. 5, respectively. As a result, the proposed metalens shows the good focusing phenomenon at a predefined position (660 μm of focal length) for both LP and CP of the incident wave. Based on Fig. 4 and Fig. 5, we can observe that the results under YLP and RCP incident waves are the same as XLP and LCP incident waves, respectively. Therefore, the polarized property of the incident wave has no influence on the focusing effect of the proposed metalens. It indicates that the proposed metalens can operate for both LP and CP of the incident wave.

Finally, the performance of the proposed metalens is compared with the previous ones. Table 3 presents the metalenses' characteristics in terms of the operating wavelength, suitable for polarized incident waves, numerical aperture, and focal spot size. It is noticed that the previous ones are not polarization insensitive, while the proposed metalens can operate for both linear polarization and circular polarization of incident wave. In addition, the proposed metalens has highest numerical aperture (NA = 0.99) that can provide sub-wavelength focal spot size ($0.54\lambda = 89\ \mu$m) near diffraction-limited ($\frac{\lambda_{operating}}{2NA}$). Compared to these previous studies [49], [50], [51], [54], [57], [63], the proposed metalens has the highest spatial resolution. Therefore, it can be very well suited for some practical applications that have a requirement matching

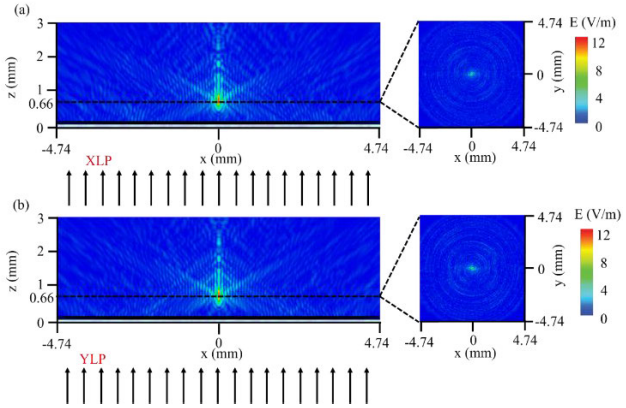

FIGURE 4. (a)-(b) The simulated intensity distribution of the metalens under XLP, YLP of the incident wave ($\lambda = 165\mu m$), respectively.

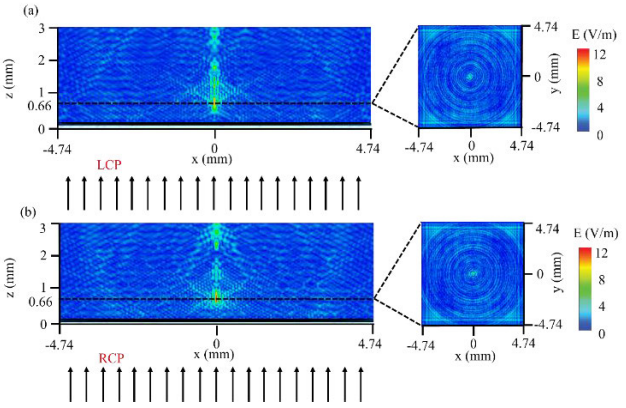

FIGURE 5. (a)-(b) The simulated intensity distribution of the metalens under LCP, RCP of the incident wave ($\lambda = 165\mu m$), respectively.

its characteristic and performance, such as terahertz imaging in cancer detection application. Although the proposed metalens has improved high spatial resolution, its fundamental transmission efficiency is not high enough for practical applications due to the large intrinsic loss of the metal material at high frequency. Moreover, increasing numerical aperture (NA) leads to decreasing efficiency. To improve the efficiency of the proposed metalens, all dielectric material should be used to obtain the high efficiency in transmission metalens type [50], [67], [68]. Recently, adding cavities inside the metallic metalens and increasing number of metal layer have reported to enhance the efficiency of the metallic metalens [69], [70].

Moreover, it should be noted that our design structure has the unit cell dimension of 80 μm × 80 μm × 90.2 μm formed of two thin layers, which is a suitable form for manufacturing with the conventional micro- and nano-technology. The proposed structure can be patterned by photolithography, while the thin film of aluminum is deposited on pre-patterned substrate using a simple thermal evaporation deposition technique and the polyimide layers are spin coated. The fabrication process of a similar THz metalens was also reported in [63]. Although microfabrication is currently in tremendous

TABLE 3. The performance comparison of the previous metalenses to this work.

References	Operating wavelength (λ)	Suitable for polarized incident wave	NA	Focal spot size FWHM (μ)	Type of article
Jia et al., 2017 [49]	96 μm	LP	0.16	6.53λ	Simulation + Fabrication
Jiang et al., 2018 [50]	119 μm	CP	0.707	1.28λ	Fabrication
Cheng et al., 2019 [51]	375 μm	CP	0.385	1.36λ	Simulation + Fabrication
Yu et al., 2021 [63]	272 μm	LP	0.95	0.76λ	Simulation + Fabrication
Wang et al. 2019 [54]	349 μm	LP	0.43	1.003λ	Simulation
He et al., 2016 [57]	375 μm	LP	0.53	0.94λ	Simulation + Fabrication
Jiang et al., 2023 [71]	166 μm	CP	0.62	0.72λ	Simulation
Qin et al., 2022 [72]	300 μm	LP, CP	0.46	0.98λ	Simulation
Hong et al., 2020 [73]	300 μm	LP, CP	0.5	0.66 λ along x direction 0.44 λ along y direction	Simulation
Jiang et al., 2024 [74]	187.5 μm	CP	0.6	0.82 λ	Simulation
This work	**165 μm**	**LP, CP**	**0.99**	**0.54λ**	**Simulation**

development, fabrication errors still occur in the metasurface fabrication. In recent years, the effects of various common fabrication errors, such as the critical dimension bias error, on the performances of metasurface in the visible, near infrared, and mid-infrared regions have been studied [75], [76], [77]. Inspired by these works, the influence of critical dimension bias error on the focusing properties of the proposed metalens is also investigated. Specifically, the impact of the ring width deviation on the focusing properties was explored via simulation. In the proposed structure, the width of the ring (W) in each proposed unit cell is set as 5 μm. The fabrication errors of the ring width are assumed to be ± 2 μm (W = 3 μm and W = 7 μm, respectively). Due to the dimension change of the ring width, the amplitude and phase of the designed unit cells will be varied. Specifically,

TABLE 4. The summary of the fabrication error results.

Fabrication error percentage	40%	0% (The designed value)	40%
Metalens with ring width W (μm)	3	5	7
Operating wavelength	165 μm (1.82 THz)		
Electric field intensity (V/m)	10.67	11.87	13.76
FWHM (μm)	0.69λ (115 μm)	0.54λ (89 μm)	0.49λ (81 μm)
Focal length (mm)	0.66	0.66	0.66
NA	0.99	0.99	0.99

the transmission amplitude of the unit cells with different ring widths is illustrated in Table S2 and Fig. S4. It is noted that the transmission amplitude of each unit cell with the ring width of 3 μm and 7 μm is tiny changed compared to the design value (5 μm). However, the mean value of transmission amplitude is maintained as 0.2 in three cases. In addition, Fig. S5 shows the phase shift of each unit cell with different ring width. It can be seen that the phase shift of each unit cell is parallel to each other around the operating frequency of 1.82 THz in three cases. It indicates that there also exists a phase shift gradient among eight-unit cells with the ring width 3 μm and 7 μm. Therefore, the metalens designing from the unit cell with the ring width (3 μm or 7 μm) can work as the proposed metalens (ring width of 5 μm). It means that they also have a focusing effect at the predefined focal length (0.66 mm).

To demonstrate the abovementioned, two other metalenses with the ring width of the unit cell (3 μm and 7 μm) are simulated, as depicted in Fig. S6 and Fig. S9. It is noted that the position of the unit cells and the simulated condition are not changed compared to the proposed metalens. Fig. S7 and Fig. S10 present the phase shift of the eight-unit cells of the two above metalenses, respectively. It is clear that the eight-unit cells can cover a full phase range from 0 to 2π. In addition, the phase shift gradient is maintained at the operating frequency of 1.82 THz. Fig. S8 and Fig. S11 present the electric field intensity distribution of the two above metalenses in the x-z and x-y planes, respectively. They indicate that these metalenses also have good focusing effect at the prescribed focal length. Moreover, the NA of these metalenses is maintained to be 0.99 despite the fabrication error is assumed as a large deviation in the ring width ($\pm$ 2μm). In addition, the focus intensity of metalens with the 3 μm ring width (10.67 V/m) is less than the proposed metalens (11.87 V/m). From the Fig. S8, the electric field intensity is extracted and the FWHM with the 3 μm could be estimated as 0.69λ. Meanwhile, the metalens with the 7 μm ring width shows a larger focus intensity (13.76 V/m) compared to the proposed metalens. Based on the Fig. S11, the electric field intensity is also extracted and the FWHM of the metalens with the 7 μm ring width could be calculated as 0.49λ. The summary of the fabrication error results is presented in Table 4. Although there is a slight deviation of the focus intensity among the metalenses with different ring widths, these values are not significantly different. In addition, the metalenses with fabrication error still maintain the high spatial resolution with sub-wavelength scale (0.69λ and 0.49λ for the metalenses with the ring width of 3 μm and 7 μm, respectively). This demonstrates the proposed metalens can be robust against this type of manufacture error.

IV. CONCLUSION

We proposed an ultrathin, polarized independent, and high numerical aperture metalens consisting of an array of DSRR and analyzed its performance through numerical simulation. The simulation results show that the proposed metalens can focus with a short focal length of 660 μm at 1.82 THz. Furthermore, the metalens using the DSRR structures can achieve a high numerical aperture (0.99) with 89 μm (0.54**λ**) of full width at half maximum (FWHM) of field distribution that leads to high spatial resolution. With outstanding properties such as planar, ultra-thin, and high spatial resolution, the suggested metalens can be served as an objective lens for miniaturized microscopy, opening a new avenue for microscopic THz imaging and showing potential usage in tiny THz imaging systems for cancer detection application.

APPENDIX

See Supplementary file for supporting content.

ACKNOWLEDGMENT

(Jong-Mo Seo and Kyo-In Koo contributed equally to this work.)

REFERENCES

[1] N. B. Lawler, D. Ho, C. W. Evans, V. P. Wallace, and K. S. Iyer, "Convergence of terahertz radiation and nanotechnology," *J. Mater. Chem. C*, vol. 8, no. 32, pp. 10942–10955, 2020, doi: 10.1039/D0TC01716G.

[2] P. R. Whelan, B. Zhou, O. Bezencenet, A. Shivayogimath, N. Mishra, Q. Shen, B. S. Jessen, I. Pasternak, D. M. A. Mackenzie, and J. Ji, "Case studies of electrical characterisation of graphene by terahertz time-domain spectroscopy," *2D Mater.*, vol. 8, Feb. 2021, Art. no. 022003.

[3] G. Wang, F. Zhu, T. Lang, J. Liu, Z. Hong, and J. Qin, "All-metal terahertz metamaterial biosensor for protein detection," *Nanosc. Res. Lett.*, vol. 16, no. 1, p. 109, Jun. 2021.

[4] Q. Sun, Y. He, K. Liu, S. Fan, E. P. J. Parrott, and E. Pickwell-MacPherson, "Recent advances in terahertz technology for biomedical applications," *Quant. Imag. Med. Surg.*, vol. 7, no. 3, pp. 345–355, Jun. 2017.

[5] G. Valušis, A. Lisauskas, H. Yuan, W. Knap, and H. G. Roskos, "Roadmap of terahertz imaging 2021," *Sensors*, vol. 21, no. 12, p. 4092, Jun. 2021.

[6] E.-M. Stübling, A. Rehn, T. Siebrecht, Y. Bauckhage, L. Öhrström, P. Eppenberger, J. C. Balzer, F. Rühli, and M. Koch, "Application of a robotic THz imaging system for sub-surface analysis of ancient human remains," *Sci. Rep.*, vol. 9, no. 1, p. 3390, Mar. 2019.

[7] M. Wan, J. J. Healy, and J. T. Sheridan, "Terahertz phase imaging and biomedical applications," *Opt. Laser Technol.*, vol. 122, Feb. 2020, Art. no. 105859.

[8] M. Danciu, T. Alexa-Stratulat, C. Stefanescu, G. Dodi, B. I. Tamba, C. T. Mihai, G. D. Stanciu, A. Luca, I. A. Spiridon, L. B. Ungureanu, V. Ianole, I. Ciortescu, C. Mihai, G. Stefanescu, I. Chirilă, R. Ciobanu, and V. L. Drug, "Terahertz spectroscopy and imaging: A cutting-edge method for diagnosing digestive cancers," *Materials*, vol. 12, no. 9, p. 1519, May 2019.

[9] H. Chen, T.-H. Chen, S.-C. Fu, W.-J. Lee, T.-F. Tseng, J.-T. Lu, Y.-F. Tsai, Y.-Y. Huang, E. Y. Chuang, Y.-J. Hwang, and C.-K. Sun, "In vivo THz fiber-scanning mammography of early breast cancer in mice," in *Proc. Int. Conf. Infr., Millim., THz Waves*, Oct. 2011, pp. 1–3.

[10] B. C. Q. Truong, A. J. Fitzgerald, S. Fan, and V. P. Wallace, "Concentration analysis of breast tissue phantoms with terahertz spectroscopy," *Biomed. Opt. Exp.*, vol. 9, no. 3, pp. 1334–1349, 2018.

[11] C. S. Joseph, A. N. Yaroslavsky, V. A. Neel, T. M. Goyette, and R. H. Giles, "Continuous wave terahertz transmission imaging of nonmelanoma skin cancers," *Lasers Surg. Med.*, vol. 43, no. 6, pp. 457–462, Aug. 2011.

[12] B. St. Peter, S. Yngvesson, P. Siqueira, P. Kelly, A. Khan, S. Glick, and A. Karellas, "Development and testing of a single frequency terahertz imaging system for breast cancer detection," *IEEE J. Biomed. Health Informat.*, vol. 17, no. 4, pp. 785–797, Jul. 2013.

[13] T. C. Bowman, M. El-Shenawee, and L. K. Campbell, "Terahertz imaging of excised breast tumor tissue on paraffin sections," *IEEE Trans. Antennas Propag.*, vol. 63, no. 5, pp. 2088–2097, May 2015.

[14] H. H. N. Pham, S. Hisatake, O. V. Minin, T. Nagatsuma, and I. V. Minin, "Enhancement of spatial resolution of terahertz imaging systems based on terajet generation by dielectric cube," *APL Photon.*, vol. 2, no. 5, May 2017, Art. no. 056106.

[15] E. Kume and S. Sakai, "Millimeter-wave radiation from a Teflon dielectric probe and its imaging application," *Meas. Sci. Technol.*, vol. 19, no. 11, Nov. 2008, Art. no. 115501.

[16] H. Yao and S. Zhong, "Plasmonic corrugated cylinder-cone terahertz probe," *J. Opt. Soc. Amer. A, Opt. Image Sci.*, vol. 31, no. 8, p. 1856, Aug. 2014.

[17] Y. H. Lo and R. Leonhardt, "Aspheric lenses for terahertz imaging," *Opt. Exp.*, vol. 16, no. 20, p. 15991, Sep. 2008.

[18] N. V. Chernomyrdin, M. E. Frolov, S. P. Lebedev, I. V. Reshetov, I. E. Spektor, V. L. Tolstoguzov, V. E. Karasik, A. M. Khorokhorov, K. I. Koshelev, A. O. Schadko, S. O. Yurchenko, and K. I. Zaytsev, "Wide-aperture aspherical lens for high-resolution terahertz imaging," *Rev. Sci. Instrum.*, vol. 88, no. 1, Jan. 2017, Art. no. 014703.

[19] A. J. Huber, F. Keilmann, J. Wittborn, J. Aizpurua, and R. Hillenbrand, "Terahertz near-field nanoscopy of mobile carriers in single semiconductor nanodevices," *Nano Lett.*, vol. 8, no. 11, pp. 3766–3770, Nov. 2008.

[20] M. Locatelli, M. Ravaro, S. Bartalini, L. Consolino, M. S. Vitiello, R. Cicchi, F. Pavone, and P. De Natale, "Real-time terahertz digital holography with a quantum cascade laser," *Sci. Rep.*, vol. 5, no. 1, p. 13566, Aug. 2015.

[21] Y. Yu. Choporova, B. A. Knyazev, and M. S. Mitkov, "Classical holography in the terahertz range: Recording and reconstruction techniques," *IEEE Trans. THz Sci. Technol.*, vol. 5, no. 5, pp. 836–844, Sep. 2015.

[22] P. Genevet, F. Capasso, F. Aieta, M. Khorasaninejad, and R. Devlin, "Recent advances in planar optics: From plasmonic to dielectric metasurfaces," *Optica*, vol. 4, no. 1, pp. 139–152, 2017.

[23] A. Siemion, A. Siemion, M. Makowski, M. Sypek, E. Hérault, F. Garet, and J.-L. Coutaz, "Off-axis metallic diffractive lens for terahertz beams," *Opt. Lett.*, vol. 36, no. 11, pp. 1960–1962, 2011.

[24] J. Suszek, A. M. Siemion, N. Błocki, M. Makowski, A. Czerwiński, J. Bomba, A. Kowalczyk, I. Ducin, K. Kakarenko, N. Pałka, P. Zagrajek, M. Kowalski, E. Czerwińska, C. Jastrzebski, K. Świtkowski, J.-L. Coutaz, A. Kolodziejczyk, and M. Sypek, "High order kinoforms as a broadband achromatic diffractive optics for terahertz beams," *Opt. Exp.*, vol. 22, no. 3, pp. 3137–3144, 2014.

[25] A. D. Squires, E. Constable, and R. A. Lewis, "3D printed terahertz diffraction gratings and lenses," *J. Infr., Millim., THz Waves*, vol. 36, no. 1, pp. 72–80, Jan. 2015.

[26] X. Ni, S. Ishii, A. V. Kildishev, and V. M. Shalaev, "Ultra-thin, planar, babinet-inverted plasmonic metalenses," *Light, Sci. Appl.*, vol. 2, no. 4, p. e72, Apr. 2013.

[27] X. Luo, "Principles of electromagnetic waves in metasurfaces," *Sci. China Phys., Mech. Astron.*, vol. 58, no. 9, Sep. 2015, Art. no. 594201.

[28] D. Lin, P. Fan, E. Hasman, and M. L. Brongersma, "Dielectric gradient metasurface optical elements," *Science*, vol. 345, no. 6194, pp. 298–302, Jul. 2014.

[29] N. Yu and F. Capasso, "Flat optics with designer metasurfaces," *Nature Mater.*, vol. 13, no. 2, pp. 139–150, Jan. 2014.

[30] H. Phan, J. Yi, J. Bae, H. Ko, S. Lee, D. Cho, J.-M. Seo, and K.-I. Koo, "Artificial compound eye systems and their application: A review," *Micromachines*, vol. 12, no. 7, p. 847, Jul. 2021.

[31] N. Yu, P. Genevet, F. Aieta, M. A. Kats, R. Blanchard, G. Aoust, J.-P. Tetienne, Z. Gaburro, and F. Capasso, "Flat optics: Controlling wavefronts with optical antenna metasurfaces," *IEEE J. Sel. Topics Quantum Electron.*, vol. 19, no. 3, May 2013, Art. no. 4700423.

[32] C. L. Holloway, E. F. Kuester, J. A. Gordon, J. O'Hara, J. Booth, and D. R. Smith, "An overview of the theory and applications of metasurfaces: The two-dimensional equivalents of metamaterials," *IEEE Antennas Propag. Mag.*, vol. 54, no. 2, pp. 10–35, Apr. 2012.

[33] N. Yu, P. Genevet, M. A. Kats, F. Aieta, J. P. Tetienne, F. Capasso, and Z. Gaburro, "Light propagation with phase discontinuities: Generalized laws of reflection and refraction," *Science*, vol. 334, no. 6054, pp. 333–337, 2011.

[34] D. Wen, F. Yue, W. Liu, S. Chen, and X. Chen, "Geometric metasurfaces for ultrathin optical devices," *Adv. Opt. Mater.*, vol. 6, no. 17, Sep. 2018, Art. no. 1800348.

[35] Y. Hu, X. Luo, Y. Chen, Q. Liu, X. Li, Y. Wang, N. Liu, and H. Duan, "3D-integrated metasurfaces for full-colour holography," *Light, Sci. Appl.*, vol. 8, no. 1, p. 86, Sep. 2019.

[36] G. Zheng, N. Zhou, L. Deng, G. Li, J. Tao, and Z. Li, "Full-space metasurface holograms in the visible range," *Opt. Exp.*, vol. 29, no. 2, pp. 2920–2930, 2021.

[37] W. Wan, J. Gao, and X. Yang, "Full-color plasmonic metasurface holograms," *ACS Nano*, vol. 10, no. 12, pp. 10671–10680, Dec. 2016.

[38] H.-T. Zhou, W.-X. Fu, Y.-F. Wang, Y.-S. Wang, V. Laude, and C. Zhang, "Ultra-broadband passive acoustic metasurface for wide-angle carpet cloaking," *Mater. Design*, vol. 199, Feb. 2021, Art. no. 109414.

[39] H. Chu, Q. Li, B. Liu, J. Luo, S. Sun, Z. H. Hang, L. Zhou, and Y. Lai, "A hybrid invisibility cloak based on integration of transparent metasurfaces and zero-index materials," *Light, Sci. Appl.*, vol. 7, no. 1, p. 50, Aug. 2018.

[40] G. Palermo, K. V. Sreekanth, N. Maccaferri, G. E. Lio, G. Nicoletta, F. De Angelis, M. Hinczewski, and G. Strangi, "Hyperbolic dispersion metasurfaces for molecular biosensing," *Nanophotonics*, vol. 10, no. 1, pp. 295–314, Oct. 2020.

[41] Y. Jahani, E. R. Arvelo, F. Yesilkoy, K. Koshelev, C. Cianciaruso, M. De Palma, Y. Kivshar, and H. Altug, "Imaging-based spectrometer-less optofluidic biosensors based on dielectric metasurfaces for detecting extracellular vesicles," *Nature Commun.*, vol. 12, no. 1, p. 3246, May 2021.

[42] W. T. Chen, A. Y. Zhu, V. Sanjeev, M. Khorasaninejad, Z. Shi, E. Lee, and F. Capasso, "A broadband achromatic metalens for focusing and imaging in the visible," *Nature Nanotechnol.*, vol. 13, no. 3, pp. 220–226, Mar. 2018.

[43] J. Engelberg and U. Levy, "The advantages of metalenses over diffractive lenses," *Nature Commun.*, vol. 11, no. 1, p. 1991, Apr. 2020.

[44] F. Balli, M. A. Sultan, A. Ozdemir, and J. T. Hastings, "An ultrabroadband 3D achromatic metalens," *Nanophotonics*, vol. 10, no. 4, pp. 1259–1264, Jan. 2021.

[45] B. Xu, H. Li, S. Gao, X. Hua, C. Yang, C. Chen, F. Yan, S. Zhu, and T. Li, "Metalens-integrated compact imaging devices for wide-field microscopy," *Adv. Photon.*, vol. 2, no. 6, pp. 1–8, Nov. 2020.

[46] X. Che, Y. Yu, Z. Gao, and Q. Yuan, "A broadband achromatic alvarez metalens," *Opt. Laser Technol.*, vol. 159, Apr. 2023, Art. no. 108985.

[47] C. Xia, M. Liu, J. Wang, Y. Wang, S. Zhang, P. Lin, and T. Xu, "A polarization-insensitive infrared broadband achromatic metalens consisting of all-silicon anisotropic microstructures," *Appl. Phys. Lett.*, vol. 121, no. 16, Oct. 2022, Art. no. 161701.

[48] X. Z. Zhu, Y. Z. Cheng, F. Chen, H. Luo, and W. Ling, "Efficiency adjustable terahertz circular polarization anomalous refraction and planar focusing based on a bi-layered complementary Z-shaped graphene metasurface," *J. Opt. Soc. Amer. B, Opt. Phys.*, vol. 39, no. 3, pp. 705–712, Mar. 2022.

[49] D. Jia, Y. Tian, W. Ma, X. Gong, J. Yu, G. Zhao, and X. Yu, "Transmissive terahertz metalens with full phase control based on a dielectric metasurface," *Opt. Lett.*, vol. 42, no. 21, pp. 4494–4497, 2017.

[50] X. Jiang, H. Chen, Z. Li, H. Yuan, L. Cao, Z. Luo, K. Zhang, Z. Zhang, Z. Wen, L.-G. Zhu, X. Zhou, G. Liang, D. Ruan, L. Du, L. Wang, and G. Chen, "All-dielectric metalens for terahertz wave imaging," *Opt. Exp.*, vol. 26, no. 11, pp. 14132–14142, 2018.

[51] Q. Cheng, M. Ma, D. Yu, Z. Shen, J. Xie, J. Wang, N. Xu, H. Guo, W. Hu, S. Wang, T. Li, and S. Zhuang, "Broadband achromatic metalens in terahertz regime," *Sci. Bull.*, vol. 64, no. 20, pp. 1525–1531, Oct. 2019.

[52] J. Li, Y. Cheng, J. Fan, F. Chen, H. Luo, and X. Li, "High-efficiency terahertz full-space metasurface for the transmission linear and reflection circular polarization wavefront manipulation," *Phys. Lett. A*, vol. 428, Mar. 2022, Art. no. 127932.

[53] C. Yang, Y. Shen, Y. Xie, Q. Zhou, X. Deng, and J. Cao, "Terahertz planar lenses based on plasmonic metasurfaces," *Phys. Lett. A*, vol. 383, no. 8, pp. 789–792, Feb. 2019.

[54] J. Wang, J. Ma, Z. Shu, Z.-D. Hu, and X. Wu, "Terahertz metalens for multifocusing bidirectional arrangement in different dimensions," *IEEE Photon. J.*, vol. 11, no. 1, pp. 1–11, Feb. 2019.

[55] Q. Wang, X. Zhang, Y. Xu, Z. Tian, J. Gu, W. Yue, S. Zhang, J. Han, and W. Zhang, "A broadband metasurface-based terahertz flat-lens array," *Adv. Opt. Mater.*, vol. 3, no. 6, pp. 779–785, Jun. 2015.

[56] R. Ji, K. Chen, Y. Ni, Y. Hua, K. Long, and S. Zhuang, "Dual-focuses metalens for copolarized and cross-polarized transmission waves," *Adv. Condens. Matter Phys.*, vol. 2018, May 2018, Art. no. 2312694.

[57] J. He, J. Ye, X. Wang, Q. Kan, and Y. Zhang, "A broadband terahertz ultrathin multi-focus lens," *Sci. Rep.*, vol. 6, no. 1, p. 28800, Jun. 2016.

[58] R. Wang, J. Han, J. Liu, H. Tian, W. Sun, L. Li, and X. Chen, "Multi-foci metalens for terahertz polarization detection," *Opt. Lett.*, vol. 45, no. 13, p. 3506, Jul. 2020.

[59] W. Wang, Z. Guo, L. Ran, Y. Sun, F. Shen, Y. Li, X. Mao, B. Wang, G. Fan, and S. Qu, "Polarization-independent characteristics of the metasurfaces with the symmetrical axis's orientation angle of 45° or 135°," *J. Opt.*, vol. 18, no. 3, Mar. 2016, Art. no. 035007.

[60] W. Wang, Z. Guo, R. Li, J. Zhang, Y. Li, Y. Liu, X. Wang, and S. Qu, "Plasmonics metalens independent from the incident polarizations," *Opt. Exp.*, vol. 23, no. 13, pp. 16782–16791, 2015.

[61] S.-W. Moon, C. Lee, Y. Yang, J. Kim, T. Badloe, C. Jung, G. Yoon, and J. Rho, "Tutorial on metalenses for advanced flat optics: Design, fabrication, and critical considerations," *J. Appl. Phys.*, vol. 131, no. 9, Mar. 2022, Art. no. 091101.

[62] M. Khorasaninejad and K. B. Crozier, "Silicon nanofin grating as a miniature chirality-distinguishing beam-splitter," *Nature Commun.*, vol. 5, no. 1, p. 5386, Nov. 2014.

[63] X. Yu, Y. Shen, G. Dai, L. Zou, T. Zhang, and X. Deng, "Phase-controlled planar metalenses for high-resolution terahertz focusing," *Photonics*, vol. 8, no. 5, p. 143, Apr. 2021.

[64] Y.-Q. Liu, J. Sun, Y. Che, K. Qi, L. Li, and H. Yin, "High numerical aperture microwave metalens," *Opt. Lett.*, vol. 45, no. 22, pp. 6262–6265, 2020.

[65] W. Wang, Z. Guo, R. Li, J. Zhang, Y. Liu, X. Wang, and S. Qu, "Ultra-thin, planar, broadband, dual-polarity plasmonic metalens," *Photon. Res.*, vol. 3, no. 3, pp. 68–71, 2015.

[66] W. Li, F. Qi, Y. Wang, P. Liu, and Z. Liu, "Refractive aspherical lens for terahertz imaging," *Opt. Commun.*, vol. 433, pp. 14–17, Feb. 2019.

[67] M. Pan, Y. Fu, M. Zheng, H. Chen, Y. Zang, H. Duan, Q. Li, M. Qiu, and Y. Hu, "Dielectric metalens for miniaturized imaging systems: Progress and challenges," *Light, Sci. Appl.*, vol. 11, no. 1, p. 195, Jun. 2022.

[68] C. Qin, W. Fan, Q. Wu, and X. Jiang, "Polarization insensitive achromatic terahertz metalens based on all-dielectric metasurfaces," *Opt. Commun.*, vol. 512, Jun. 2022, Art. no. 128061.

[69] H. Li, B. Fang, C. Chen, S. Zhu, and T. Li, "Cavity-enhanced metallic metalens with improved efficiency," *Sci. Rep.*, vol. 10, no. 1, p. 417, Jan. 2020.

[70] J. Luo, H. Yu, M. Song, and Z. Zhang, "Highly efficient wavefront manipulation in terahertz based on plasmonic gradient metasurfaces," *Opt. Lett.*, vol. 39, no. 8, pp. 2229–2231, 2014.

[71] X.-Q. Jiang, W.-H. Fan, L.-R. Zhao, X. Chen, C. Qin, H. Yan, Q. Wu, and P. Ju, "Continuously varifocal metalens for broadband achromatic focusing of terahertz waves," *J. Sci., Adv. Mater. Devices*, vol. 8, no. 3, Sep. 2023, Art. no. 100560.

[72] X. Jiang, W. Fan, C. Qin, and X. Chen, "Ultra-broadband polarization conversion metasurface with high transmission for efficient multi-functional wavefront manipulation in the terahertz range," *Nanomaterials*, vol. 11, no. 11, p. 2895, Oct. 2021, doi: 10.3390/nano11112895.

[73] X. Hong, S. Feng, H. Guo, and C. Li, "A small-spot-size and polarization-insensitive flat lens employing dielectric metasurface in the terahertz region," *Opt. Commun.*, vol. 459, Mar. 2020, Art. no. 125083.

[74] Z. Jiang, M. Chao, Q. Liu, B. Cheng, G. Song, and J. Liu, "High-efficiency spin-selected multi-foci terahertz metalens," *Opt. Lasers Eng.*, vol. 174, Mar. 2024, Art. no. 107816.

[75] A. Patoux, G. Agez, C. Girard, V. Paillard, P. R. Wiecha, A. Lecestre, F. Carcenac, G. Larrieu, and A. Arbouet, "Challenges in nanofabrication for efficient optical metasurfaces," *Sci. Rep.*, vol. 11, no. 1, p. 5620, Mar. 2021.

[76] Y. Zhu, W. Wang, F. Yu, Q. Liu, Z. Guo, G. Li, P. Chen, and W. Lu, "The impact of manufacturing imperfections on the performance of metalenses and a manufacturing-tolerant design method," *Micromachines*, vol. 13, no. 9, p. 1531, Sep. 2022, doi: 10.3390/mi13091531.

[77] G. Xu, Q. Kang, X. Fan, G. Yang, K. Guo, and Z. Guo, "Influencing effects of fabrication errors on performances of the dielectric metalens," *Micromachines*, vol. 13, no. 12, p. 2098, Nov. 2022, doi: 10.3390/mi13122098.

HUU LAM PHAN received the B.S. degree from the School of Electronics and Telecommunications, Vinh University, Vietnam, in 2016, and the Ph.D. degree from the Department of Electrical, Electronic and Computer Engineering, University of Ulsan, Ulsan, Republic of Korea, in 2023. His current research interests include metasurfaces-based metalens, polarization converters, and absorber.

KWANGSOO KIM received the B.S., M.S., and Ph.D. degrees in electrical engineering from Seoul National University, Republic of Korea, in 1996, 1998, and 2004, respectively. He was a Senior Researcher with Samsung Electronics, from 2004 to 2007, and the Manager with Hyundai Motor Company, from 2007 and 2008. In 2008, he joined the Department of Electronic Engineering, Hanbat National University, Republic of Korea, where he is currently a Professor. His current research interest includes machine learning for computer vision and control.

JONG-MO SEO (Member, IEEE) received the B.S., M.S., and Ph.D. degrees from the College of Medicine, Seoul National University, Seoul, Republic of Korea, in 1996, 2002, and 2005, respectively. Since 2008, he has been an Associate Professor with the School of Electrical Engineering and Computer Science, Seoul National University. His research interests include artificial vision and various vitreo-retinal diseases.

KYO-IN KOO (Member, IEEE) received the B.S. and Ph.D. degrees in electrical engineering from Seoul National University, Republic of Korea, in 2003 and 2009, respectively. In 2013, he joined the Department of Biomedical Engineering, School of Electrical Engineering, University of Ulsan, Ulsan, Republic of Korea, where currently an Associate Professor. His current research interests include the meta-material and the three-dimensional bio-printing for biomedical applications.